Int. J. Advanced Design and Manufacturing Technology, 2025, Vol. 18, No. 1, pp. 37-49

DOI: 10.71644/admt.2025.1121450 ***ISSN: 2252-0406*** ***https://admt.isfahan.iau.ir***

Analyzing the Dynamic Performance of the Two-Stage Pusher Centrifuge

Mehdi Jafari Vardanjani*, Hamed Barghikar
Department of Mechanical Engineering,
National University of Skills (NUS), Tehran, Iran
E-mail: m-jafari@nus.ac.ir, hbarghikar@nus.ac.ir
*Corresponding author

Received: 1 June 2024, Revised: 9 November 2024, Accepted: 11 December 2024

Abstract: Mechanical filtration of solid and liquid phases with the help of a centrifuge mechanism is a common operation in industries, particularly for salt dehydration. The process is mainly based on the centrifuge action between particles and fluids. Currently, most of the studies have been performed on single-stage centrifuges while there it is required to know and analyze the behaviour of the multi-stage pusher centrifuges in order to optimize their efficiency. The structure and dynamic performance of the two-stage pusher centrifuge device have been analyzed in the current study in three phases: modal, particle behaviour, and transient state dynamics analysis. The results of the modal analysis have demonstrated that the safety margin obtained in the context of the resonance occurrence for the internal basket set and subset due to linear and rotational inertial forces has been 40%. Based on the results of the transient dynamics analysis, the stability of the particle behavior has been about 5.5 s or 68% of the particle feeding time, the maximum displacement at the critical point of the inner basket subset has been 0.51 mm, and the critical stress value has been about 27 MPa; which has been acceptable in terms of mechanical strength of the assembly versus the stresses and strains caused by the operation of the device. Thus, it is recommended based on the results to maintain the maximum rotational motion (36.68 rad/s) and no significant change in the particle feeding rate compared to the specified value (0.56 kg/s).

Keywords: Dynamic Analysis, Modal Analysis, Pusher Centrifuge

Biographical notes: Mehdi Jafari Vardanjani is an Assistant Professor of Mechanical Engineering at the National University of Skills (NUS), Iran. He received his PhD in Manufacturing from the University of Tehran, Iran in 2016 and his MSc from the Isfahan University of Technology, Iran. His current research interest includes vibrational effects in mechanics and manufacturing processes. **Hamed Barghikar** is an Assistant Professor of Mechanical Engineering at the National University of Skills (NUS), Iran. He received his PhD in Manufacturing from the Isfahan University of Technology, Iran in 2018, and his MSc from the Isfahan University of Technology, Isfahan, Iran. His current research interest includes machining, metal forming, and polymer processing.

Research paper

1 INTRODUCTION

Mechanical filtration of solid and liquid phases is a common operation in industries including chemical, pharmaceutical, wastewater treatment, and food industries [1]. In this regard, centrifuges are used for a wide range of applications, the most common of which is related to dewatering [2]. Pusher centrifuge device is used for dewatering, drying, and separating materials (fibers, crystals, and powders) continuously. Input mixture enters the centrifuge through the feed pipe and is distributed uniformly inside the centrifuge basket when it goes to the distributor. Then the solid phase formed on the basket can be washed away by water jets. In fact, the dehydration process is done by the centrifugal force created in the centrifuge while the discharge of the dried solid phase is done. Therefore, the performance of the device is influenced by parameters such as the rotational balance of the device during material feeding, dewatering, and separation operations, and the static strength. Thus, the performance of the device is considerably influenced by the feeding rate of materials and their circulation during the working cycle. These parameters also affect the depreciation and noise pollution of the device. Therefore, it is crucial to analysis the structure and dynamic performance of the device.

Bowl and tube centrifuges are used for the effective separation of fine solids due to their high centrifugal acceleration [3]. Sedimentation might also occur during the centrifugal process. The rheological behavior of the sediments affects its shape. However, the shape of the deposit has a significant effect on the flow conditions inside the centrifuge. This affects the efficiency and speed of the separation [4]. The performance of centrifuges has been evaluated in the initial studies based on the Sigma method [5]. In this method, the complexity of turbulent flow conditions and growing sediments are ignored. This causes discrepancies between the results of the evaluation of separation performance in practice and theoretical discussions [3].

Some studies have performed a complete analysis of the flow conditions in centrifuges based on computational fluid dynamics simulation. In this regard, various types of approaches have been observed for simulating turbulent multiphase flows. The approaches used in this field include standard and computational fluid dynamics (CFD) methods developed by researchers [6]. According to the analyzes carried out in the field of separation, it was determined that the examination of the separation process in shell and semi-continuous centrifuges is somewhat dependent on the simulation of the flow conditions. It should be mentioned that the use of simplified models to investigate the different flows of particles and liquids, along with the investigation of the sedimentation effects, have also provided favorable and appropriate results [7].

Since complex multiphase flows occur in the centrifuges, the arrangement of the centrifuge machine parts, process control parameters, and material properties affect the flow paradigm. Although to design a centrifuge or its mechanical separation process, it is necessary to know the flow conditions, the experimental investigation of the flow inside the centrifuges is very complicated. Therefore, CFD is a suitable alternative to practical testing. In this regard, Bürger and colleagues [7] investigated the sediment formation process using a simple approach in centrifuges. In this analysis, the settling behavior of materials is described only by the flux density function. The numerical results have shown a good agreement with the experimental results of a centrifugal process.

Romani et al [3] investigated the sedimentation process in a solid bowl centrifuge with Euler-Lagrangian characteristics. The flow of all three phases in centrifuges is directly resolved spatially and temporally, which requires a long time to perform calculations. Therefore, a period of time has been considered to analyze this trend. In general, the methods used in the previous studies in the past research considered compromises between all the results and the calculation time, which is a normal procedure.

Although there has been extensive research in the field of bowl and tube centrifuges, and the fluid laws that govern them, the topic of two-stage and multi-stage separator pusher centrifuges has rarely been analyzed [8]. Two-stage centrifuges are among the separating centrifuges whose discharge is done in stages that allow continuous operation. In these centrifuges, all steps of separation, washing, drying, and depletion can be done at the maximum speed of the device. In addition to designing a suitable structure, these centrifuges have a low power consumption, high capacity, and the capability to extract materials continuously and maintain humidity in low amounts. Therefore, this device is used in many chemical industries to separate materials from heterogeneous phases and dehydrate mixtures containing crystals or fibrous solids [9].

Currently different theoretical researches have been done on two-stage pusher centrifuges. The main reason for this issue is the complexity and variety of centrifuge separation processes. Mainly, the inability to determine the dimensions, shape, and movements of particles accurately due to the irregular conditions created on them, makes complex mathematical problems. This issue leads to difficulties in conducting theoretical studies of this process. On the other hand, parameter optimization based solely on experimental tests is not very reliable and costly. Therefore, in order to determine the laws governing fluid flow in the centrifuge process, appropriate mathematical models can be developed [10]. For spatial and temporal numerical simulations, an approach based on the fast Eulerian-Ferry method [11] has been devised to achieve a balance between the required physical accuracy and calculation time. In this method, the solid phase (desired salt powder particles) and the liquid phase are approximated as a mixed phase. Therefore, in order to consider the effect of different conditions of the flow behavior of the desired mixture, the average spatial and temporal viscosity of the fluid and the average size of the particles have been considered. The velocity field $v(\vec{x},t)$ for the mixed phase is calculated by solving Navier-Stokes Equation s. $\vec{x}$ is the position in space, and t is time. The particle velocity field ($v_p(\vec{x},t)$) can be evaluated based on the mixed phase velocity field $v(\vec{x},t)$ and the spatial settling velocity v_{Bulk}. This reduces the solution time compared to the classical Eulerian method. In this regard, a temporary spatial viscosity ($\eta_{MP}(\vec{x},t)$) was used in order to consider the different behaviors of the mixed phase:

$$\eta_{MP}(\vec{x},t) = A \cdot \eta_{Susp}(\vec{x},t) + B \cdot \eta_{Sed}(\vec{x},t) \tag{1}$$

In the above Equation , $\eta_{MP}(\vec{x},t)$ is calculated based on the viscosity of the mixture ($\eta_{Susp}(\vec{x},t)$) and virtual viscosity of the settling material ($\eta_{Sed}(\vec{x},t)$). A is the mixing coefficient and B is the sediment spatial coefficient. The values of A and B change between the values of 0 and 1 depending on the type of phase, depending on whether the phase is mixed or settled. Although coefficients have been used in this study to simplify the mixture analysis process and to investigate its behavior, the presented solution can be considered and even used to advance the goals of analysis and simulation.
In the present study, the analysis of the structure and dynamic performance of the two-stage pusher centrifuge device has been demonstrated. In this regard, the simulation task has been considered for the subsets of the inner basket, the outer basket, and the feeding chamber in three phases: modal analysis, particle behavior analysis, and transient state dynamics analysis. Finite element analysis results have been analyzed and compared with the experimental results.

2 METHODS

The 3-dimensional (3D) modelling and finite element analysis (FEA) procedure are explained here.

2.1. 3D Modelling

The intended set ("Fig. 1") was designed as the inner basket subset, outer basket subset, rotating disc, and feeding shell according to Ferrum-P-32 model pusher centrifuge geometry.
"Table 1" lists the parts in the created design.

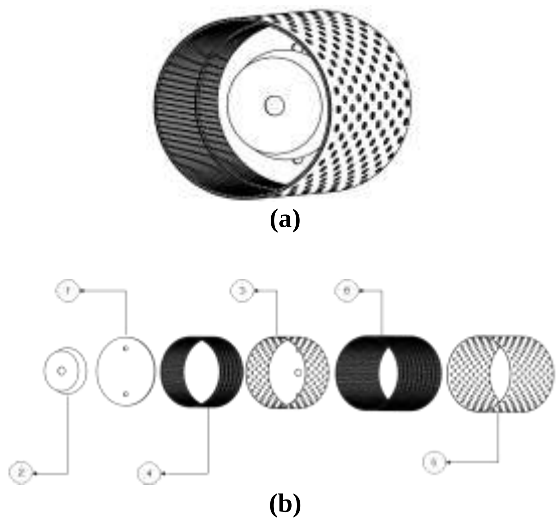

Fig. 1 3D model designed for finite element analysis; (a) Assembly; (b) Exploded view.

Table 1 List of parts of the 3D model designed

Number	Part Number	Type	Quantity
	SA-Basket-1	Assembly	1
	SA-Basket-2	Assembly	1
1	Rotating-Disk	Part	1
2	Cover	Part	1

Bill of Material: SA-Basket-1

Number	Part Number	Type	Quantity
3	Basket-1	Part	1
4	Wedge-Wire-1	Part	1

Bill of Material: SA-Basket-2

Number	Part Number	Type	Quantity
5	Basket-2	Part	1
6	Wedge-Wire-2	Part	1

2.2. Simulations

The desired dynamic analysis is done in two separate categories: modal analysis and transient dynamic analysis.

2.2.1. Modal Analysis

The preparatory steps including the boundary conditions and connections for the complete set and members can be defined as follows:

2.2.1.1. The Complete Set

Figure 2-a shows the model used to perform modal analysis for the entire configuration. In order to perform modal analysis in the software, boundary conditions, and connections were applied on the set and members according to “Fig 2-b”. The material used for the members was stainless AISI 304. The chemical composition of this steel is mentioned in “Table 2”and its important physical and mechanical properties are mentioned in “Table 3”.

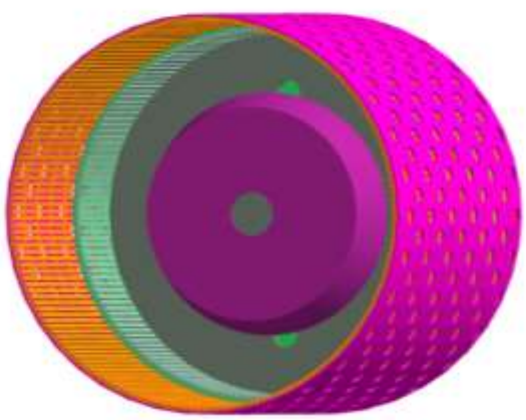

(a)

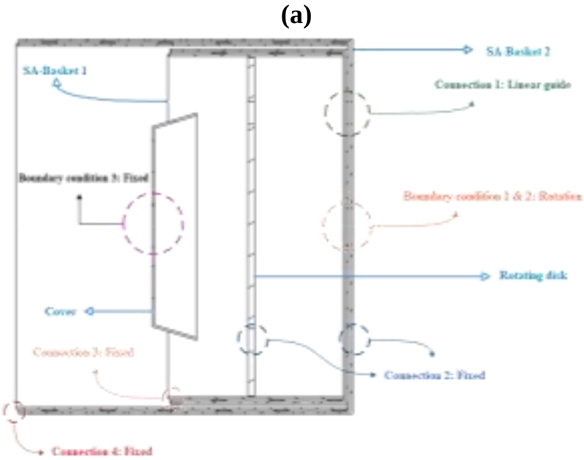

(b)

Fig. 2 Schematics of the model used for modal analysis: (a): 3D model of the assembly, and (b): The cut view of the model along with the display of connections and boundary conditions (The wedge-wires are depicted in a simple form for simplicity of the display.)

Table 1 Chemical composition of AISI 304 steel used for components

Element	Percent		
C	0	-	0.08
Cr	18	-	20
Fe	65.8	-	74
Mn	0	-	2
Ni	8	-	11
P	0	-	0.045
S	0	-	0.03
Si	0	-	1

Table 3 Physical and mechanical properties defined for the components

Parameter	Value
Density ($\frac{kg}{m^3}$)	7960
Elasticity modulus (MPa)	197
Yield strength (MPa)	258
Tensile strength (MPa)	565
Poison ratio	0.27
Hardness (HB)	175
Fatigue strength at 10^7 cycle (MPa)	241

2.2.1.2. The Inner Basket Sub-Set

The imported model of the inner basket sub-set (including wedge-wire and basket) can be seen in “Fig. 3”. This sub-set has also been subjected to modal analysis separately.

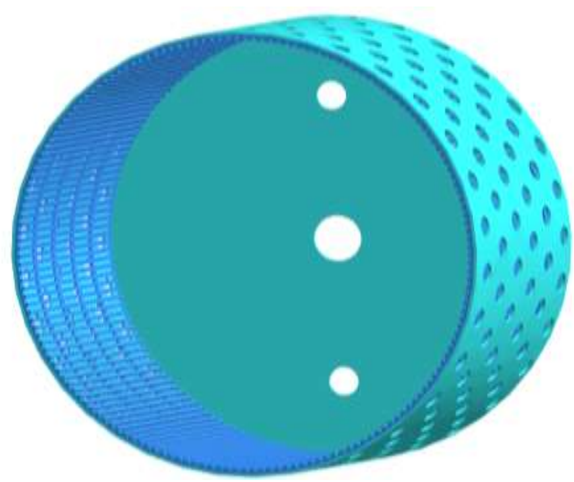

Fig. 32 Inner basket subset model.

2.2.2. Dynamic Behavior Analysis

Different available methods have been evaluated initially to choose the appropriate one in terms of practicality and precision. Since the input and output materials of the machine are both in the form of granular materials (powder), the following can be mentioned as different approaches to perform such an analysis:

- Flexible dynamic along with fluid dynamics analysis: this method is one of the most complex and time-consuming approaches that can be used here. Although in terms of assumptions, this method is closer to reality, the flexible dynamics of the desired member due to the relatively complex geometry of the wedge-wire, make it almost impossible to solve. In addition, the simultaneous calculation of fluids to investigate the behavior of salt powder would be another difficulty during the task.

- Flexible dynamic and fluid dynamics analysis separately: in this method, simulation is performed once in the form of rigid body dynamics to check the dynamic behavior of particles. This way, the number of contacts, pressure distribution, and the effect of random load caused by particles on the target member are obtained. Therefore, it is possible to extract the dynamic unbalanced load behavior caused by the particles and use it to find the load function of these particles on the desired member. Nevertheless, it should be noted that this loading function is dependent on the time and position inside the member. It is also necessary to mention that the duration of stability of particle behavior is obtained in fluid dynamics analysis. In other words, since the member starts moving from the stationary state until it reaches a constant speed, it will not be a definitive criterion for the stability of the behavior of this function; Rather, the duration of stability of the load behavior should be obtained according to the dynamic analysis and the particle outlet rate.
- Flexible dynamic and and discrete dynamic analysis of particles separately: this approach is the same as the previous approach, with the difference that the discrete method has been used to simulate powder and independent particles. Although this method is more compatible with the target problem, the solution of both methods will be relatively the same.
- Using the third method, the intended steps could be summarized as follows:
  - Discrete element simulation of particles
  - Extracting the loading function (stress distribution)
  - Transient state dynamics analysis
  - Extraction of mechanical parameters including distribution of stress and strain on the desired member

2.2.2.1. Discrete Elements Analysis of Particles

In order to simulate the dynamic behavior of powder particles, EDEM Rocky software was used as a discrete element analysis simulation tool. The steps are briefly described below:

- 3D Model

Figure 4 demonstrates the imported set to simulate the behavior of particles in the software.

- Feeding chamber

In order to simplify the solution and the possibility of repeating the simulation and modification, the complexities in the geometry of some components such as bolts and nuts are omitted and some components such as the guide bushings and coupling are not included in the model. Nevertheless, the function of these components is defined in the model. The inlet port of the feeder is defined with a diameter equal to the diameter of the shell of the feeder section according to “Fig. 5”.

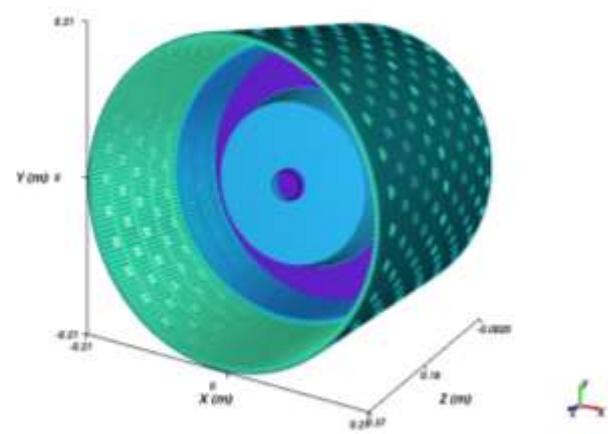

Fig. 4 The entire model used in the simulation software to check the behavior of particles.

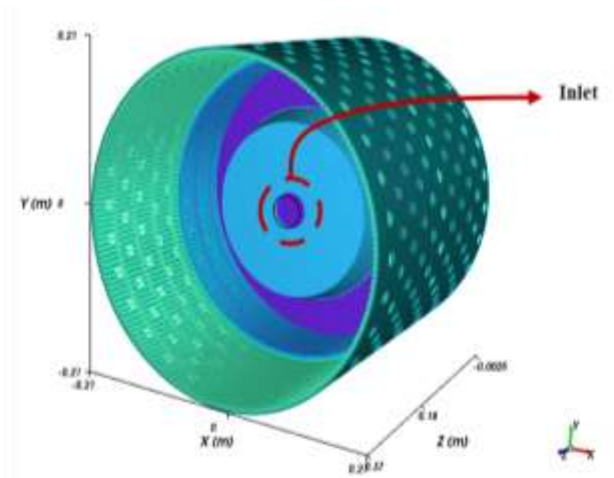

Fig. 5 Feeding inlet port in the model

Table 4 demonstrates the specifications applied in the software for feeding inlet. It should be noted that the concentration of particles in the water fluid is 18% and the feeding beginning time is considered to be at 8 s.

- Movements definitions

The required rotational and oscillating motions were applied to the disk, the inner basket subset, and the outer basket subset according to the values obtained from the actual operation of the device [6], [12]. Table 5 provides the applied values.

Table 2 Specifications of the fed particles inside the chamber for simulation

Parameter	Particle mass (kg)	Particle volume (m^3)	Particle density ($\frac{\mathrm{kg}}{\mathrm{m}^3}$)	Particles inlet mass flow rate ($\frac{\mathrm{kg}}{\mathrm{s}}$)	Particles inlet volume flow rate ($\frac{\mathrm{m}^3}{\mathrm{s}}$)
Value	424×10^{-6}	1.96×10^{-7}	2163	0.56	2.6×10^{-4}

Table 3 The values of the kinematic parameters applied for the components of the simulation

Part (subset)	Rotational speed ($\frac{\mathrm{rad}}{\mathrm{s}}$)	Reciprocation frequency (Hz)	Amplitude (m)
Rotating disk	36.65	0	0
Feeding shell	0	0	0
Inner basket subset	36.65	0.5	0.025
Outer basket subset	36.65	0	0

- Particle sedimentation rate

In order to take into account the particle sedimentation caused by centrifugal force in the fluid, the results of Reynold and Sokolov experiments [6] were used to investigate the behavior of particles during the simulation process and convert them into filtered mass (cake). According to the results of these experiments, the sedimentation speed (u) can be expressed as follows in the radius r of a turbulent area in terms of $\frac{m^3}{s}$:

$$u(r) = 1.75\,\eta_1 \left[\frac{d\omega^2 r(\rho_s - \rho_l)}{\rho_l}\right]^{0.5} \tag{2}$$

Where:

$$\eta_1 = (1 - x_s)^{5.5} \tag{3}$$

Where η_1 is the settling speed correction factor, x_s is the ratio of solid (powder) to mixture, d is the average diameter of the particles, ρ_l is the density of the liquid, ρ_s is the density of the solid (powder), and ω is the angular velocity of the liquid in radius r. The speed (ω) can be calculated using the following Equation [6]:

$$\omega(r) = \omega_0 \left[1 - \left(\beta \times \frac{Q}{\nu^{0.5} \cdot r_1}\right) \cdot \frac{\left(\frac{r_2}{r}\right)^2 - 1}{\left(\frac{r_2}{r_1}\right)^2 - 1}\right] \tag{4}$$

Where ω_0 is the angular velocity of the basket, r_1 is the radius of the free surface, r_2 is the radius of the basket wall (wedge-wire), Q is the inlet flow rate of the fluid mixture and powder, ν is the kinematic viscosity of the liquid, and $\beta = 2.6 \times 10^{-7} \frac{\sqrt{s}}{m}$. α is a constant coefficient assumed due to the nature of the fluid and algebraic simplifications of the Equation. The considered values for "Eq. (2) to (4)" are mentioned in "Table 6".

Table 4 The values considered for the "Eq. (2) to (4)" calculate the sedimentation rate of parties

Parameter	d (m)	$\rho_s \left(\frac{\mathrm{kg}}{\mathrm{m}^3}\right)$	$\rho_l \left(\frac{\mathrm{kg}}{\mathrm{m}^3}\right)$	x_s	$\omega_0 \left(\frac{\mathrm{rad}}{\mathrm{s}}\right)$	r_1 (m)	r_2 (m)	$\nu \left(\frac{\mathrm{m}^2}{\mathrm{s}}\right)$	$Q \left(\frac{m^3}{s}\right)$
Value	0.0072	2163	1000	0.2	36.65	0.18	0.1925	10^{-6}	0.002513

Figure 6 demonstrates the sedimentation rate of the particles ($u(r)$) inside the inner basket in versus radius (r). Also, according to the "Eq. (2)", the speed rates for the radius of the free surface (r_1) and maximum value (r_2) are obtained as $u(r_1) = 0.73\,\frac{m}{s}$ and $u(r_2) = 0.755\,\frac{m}{s}$, which indicates the small variation of this parameter along the radius. Therefore, the obtained changes and the sedimentation rate of the particles have a slight effect on the loading fluctuations and the imbalance of its behavior during the process. Therefore, it can be ignored with negligible error in calculations.

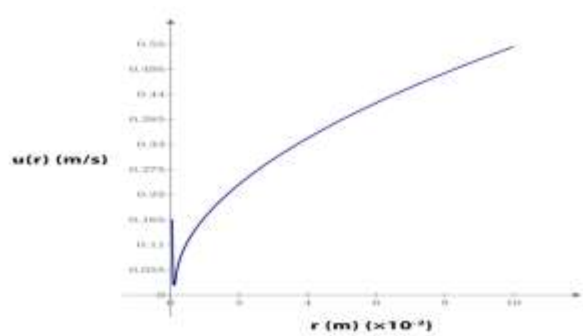

Fig. 6 Particle sedimentation rate ($\boldsymbol{u(r)}$) inside the inner basket (wedge-wire) versus radius ($\boldsymbol{r}$).

- Stress-time function

Contact spots are demonstrated 5 seconds after the beginning of the simulation (at the middle of the simulation durations) in the front view in “Fig. 7”. Although the contact points are not constant during the simulation process, it is important to check the critical points to obtain the appropriate variable stress distribution in the next stages of the simulation. Thus, in order to obtain the time-varying loading function, the regions A to D have been defined according to “Fig. 8” to retrieve average stress-time data in these regions. Figure 9 demonstrates the vertical stress variation diagram applied to region A as an example. As the diagram shows, the changes in load value have occurred in a certain range (between 0 and 5000 Pa).

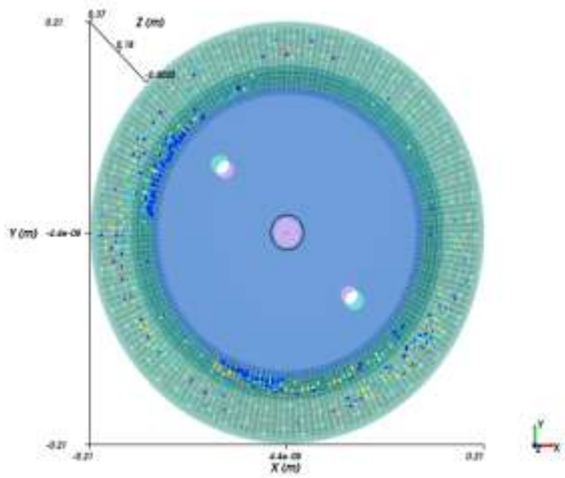

Fig. 7 The contact points of the particles and the inner basket at the middle of the simulation duration in colored dots in the front view. (For simplicity in the display, the feeding shell is hidden.)

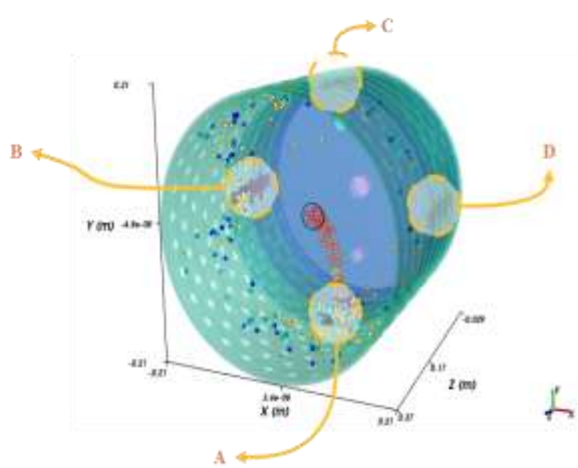

Fig. 8 Checkpoints defined to extract the average stress distribution diagram versus time (for simplicity in the display, the shell of the feeding section is hidden.)

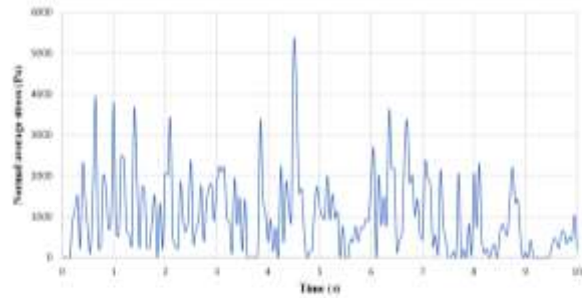

Fig. 9 An example of the average stress distribution diagram extracted in region A.

The values obtained from ranges A to D have been transformed to the stress-time table and have been indirectly applied as a coefficient of the time-dependent stress function on the inner surface of the inner basket in order to analyze the dynamic behavior in the transient state. To do this, the following steps were taken:

- Obtaining stress distribution values of each region

First, the stress distribution values of all 4 regions were obtained according to “Fig. 10” during the simulation.

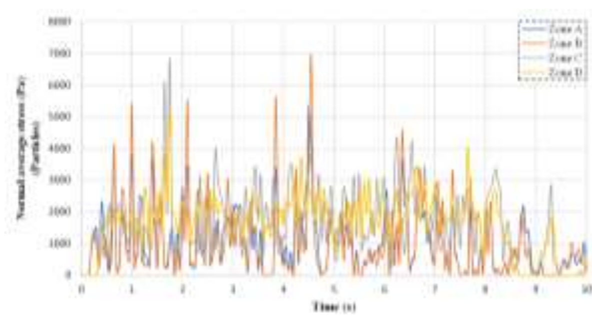

Fig. 10 Stress variations of regions A to D within the inner basket.

- Calculation of normalized values

At this step, the normalized function of the average value was obtained in the range between 0 and 1, taking into account the maximum and minimum values according to “Fig. 11”.

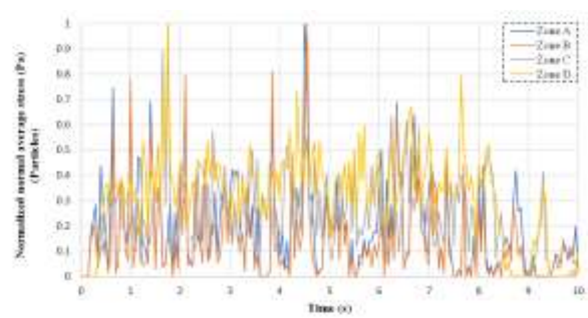

Fig. 11 Normalized values of the average stress variations in regions A to D within the inner basket.

○ Calculation of the mixture loading function

Since the powder particles are fed as a mixture with the liquid inside the assembly, the final pressure distribution will be a combination of the pressure caused by the liquid and the particles. Therefore, the final stress distribution is considered as the product of the normalized values of the stress caused by the particles in the hydraulic pressure of the centrifuge. The hydraulic pressure caused by the fluid on the basket wall can be calculated via the following Equation [13].

$$p_c = \rho\omega^2 \int_{r_1}^{R} r dr = \frac{1}{2}\rho\omega^2(R^2 - r_1^2) \tag{5}$$

Where p_c is the hydraulic pressure of the centrifuge, ρ is the density of the fluid, ω is the rotational speed of the basket, r is the radius, R is the radius of the basket, and r_1 is the radius of the free surface of the fluid. The considered values for these parameters are mentioned in "Table 7".

Table 5 The values considered for Equation (5) to calculate the stress (pressure) caused by the mixture

Parameter	$\rho\left(\frac{\mathrm{kg}}{\mathrm{m}^3}\right)$	$\omega\left(\frac{\mathrm{rad}}{\mathrm{s}}\right)$	R (m)	r_1 (m)
Value	1000	36.65	0.1925	0.18

Therefore, the distribution of stress (pressure) caused by the mixture of fluid and particles is assumed as "Fig. 12" in the transient dynamics analysis section.

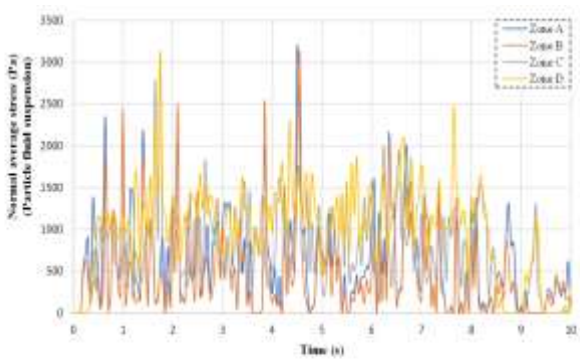

Fig. 12 The stress value versus time caused by the mixture of fluid and particles to be applied inside the inner basket subset to analyze the dynamic behavior in the transient state.

Since the diagram obtained in "Fig. 12" assumes a uniform pressure distribution in the internal space at any time, the imbalance in loading at different angle positions is not taken into account. Therefore, it is necessary to consider this imbalance somehow in the loading of different regions. In fact, the amount of load difference between the regions should be included in the values. In order to achieve this goal, the normalized value of the load distribution of each region in the diagram of "Fig. 12" has been multiplied and its product is considered as the time function required to be applied in the dynamic analysis of the transient state. In addition, in order to increase the accuracy of the analysis in the phase of transient dynamics analysis, the medial regions between the 4 initial regions have been considered and their values have been calculated by interpolating. Figure 13 shows the final arrangement of areas A to D and intermediate areas. Figure 14 exhibits the calculated final stress distribution values for the intermediate areas AB to DA.

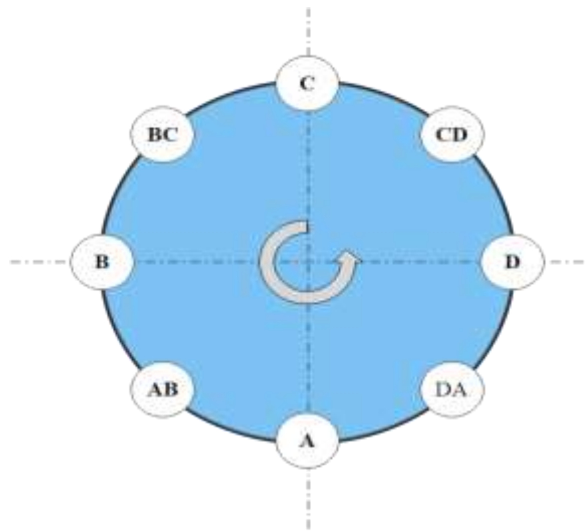

Fig. 13 The location of the regions A to D and intermediate regions (AB to DA) in the inner basket.

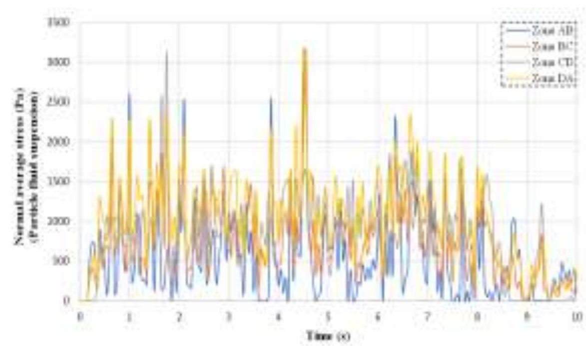

Fig. 14 Calculated values of fluid and particle mixture stress for the intermediate regions AB to DA.

2.2.2.2. Transient Dynamic Analysis

The model used to simulate the transient dynamic behavior is shown in "Fig. 2-a". The boundary conditions and connections have been similar to those mentioned in the modal analysis section ("Fig. 2b"). The kinematic and dynamic parameters are defined according to "Table 5". In order to apply the dynamic stress distribution obtained from the particle behavior analysis section, time-stress distribution functions were defined in the form of tabular functions in the regions A to D. Figures 15 & 16 show how these loads are set for area A. The aforementioned variable loading was defined for other regions AB to DA in a similar way.

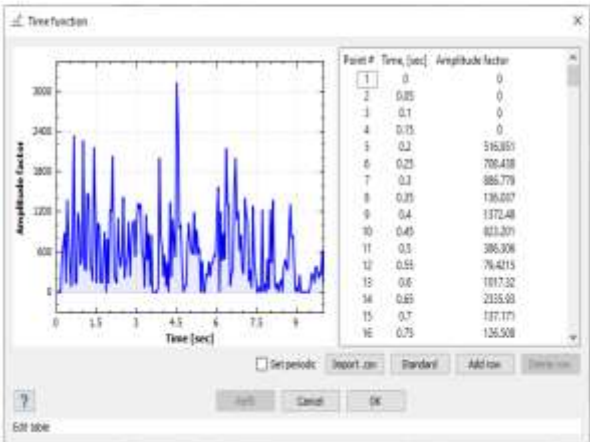

Fig. 15 The definition of the time-stress function extracted from the particle analysis section to analyze the dynamic behavior of the transient state.

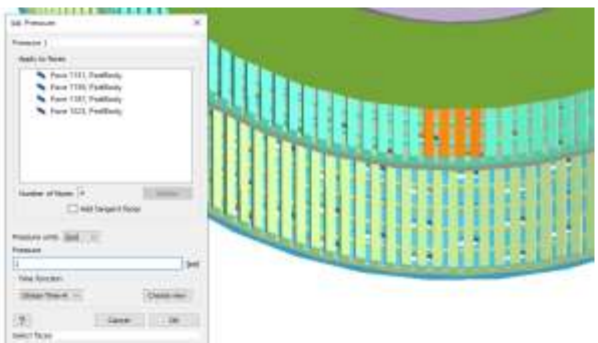

Fig. 16 Applying the time-stress function from the particle analysis section on region A to analyze the dynamic behavior of the transient state.

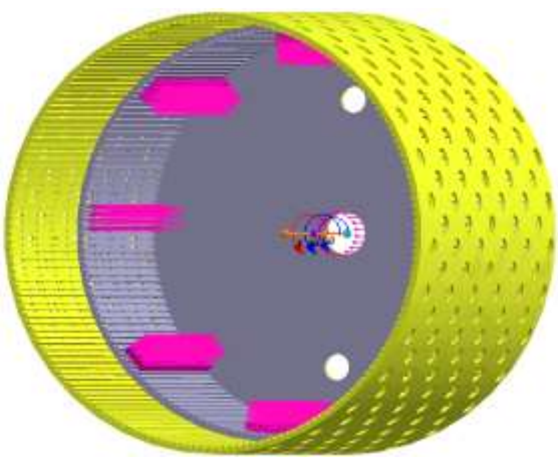

Fig. 17 The assembly with the predefined loading and reciprocating movement of the internal subset (The feeding chamber is hidden).

In order to define the rotation and the resulting inertia on the set with the desired angular velocity ("Table 5"), the angular velocity was defined for the whole set. Also, in order to define the reciprocating motion of the internal basket subset with the desired frequency ("Table 5"), an alternating sinusoidal motion on the internal basket subset was applied. Figure 17 shows the prepared assembly with applied loads and motions.

3 RESULTS AND DISCUSSION

The experimental validation of the results was assured about in range of force values and relative displacement according to previous studies conducted in this field [14-17]. According to the values obtained in these studies, the average value of the force measured due to the contact of particles with the inner surfaces of the basket differed by about 9%. Also, the difference in the average value of the relative displacement obtained in the practical test was about 4% compared to the obtained results here. The reasons for this scatter between experimental and simulation values can be related to factors such as simplifying assumptions applied in the geometry, measurement accuracy in dynamometers and strain gauges, and simplifying assumptions considered in the simulation.

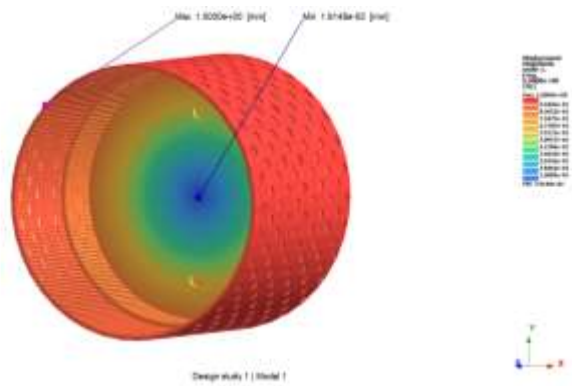

Fig. 18 The result obtained from the modal analysis performed on the assembly in mode 1 in the form of the color contour of the relative maximum displacement

3.1. Modal Analysis

The results obtained in this section include the relative displacements caused in the parts and the calculation of their natural frequency. In order to interpret the results of the modal analysis, the natural frequencies of the set and the subset of the inner basket have been compared with the normal working vibration frequency of the device. Then the resonance phenomenon for the critical mode has been investigated. The critical mode was assumed as the mode in which the maximum displacement occurred. Also, a comparison has been made between the natural frequency of the set and the subset of the internal basket. Figure 18 shows the maximum relative displacement in the first mode of the modal analysis. The results obtained for all modes are summarized in "Fig. 19". The natural frequency values for "Fig. 19" are mentioned in "Table 8".

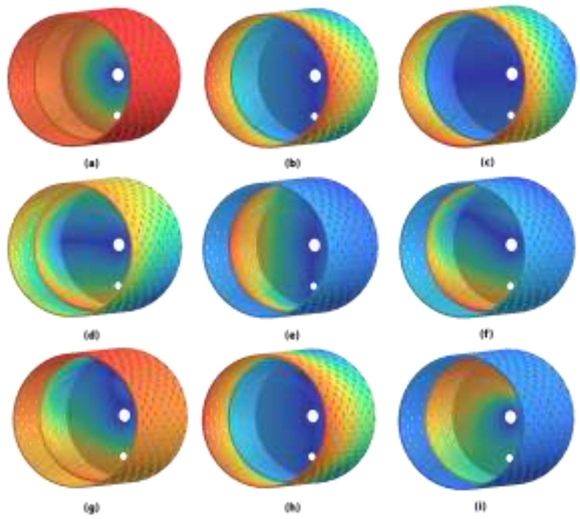

Fig. 19 The results of the modal analysis performed on the set in the form of a colored contour of the relative maximum displacement: (a): mode 1, (b): mode 2, (c): mode 3, (d): mode 4, (e): mode 5, (f): mode 6, (g): mode 7, (h): mode 8, and (i): mode 9, (The range of changes from the minimum (blue) to the maximum (red) is the same for all of the items).

Table 6 Natural frequency values in the investigated modes of the set

Mode No.	Natural frequency (Hz)	Mode No.	Natural frequency (Hz)
1	0.00	6	23.49
2	8.15	7	27.76
3	9.42	8	29.61
4	20.60	9	42.11
5	21.59		

According to the rotational speed of the device based on "Table 5" ($36.65\frac{\text{rad}}{\text{s}}$), it can be concluded that the normal working vibration frequency of the device is 5.83 Hz. According to the results found in "Fig. 19" and "Table 8", the natural frequencies of the modes are different from the normal working vibration frequency of the device. Thus, the probability of the resonance phenomenon is negligible for the set.

The relatively small difference between the vibration frequency of the device and the natural frequency in the second vibration mode ("Fig. 19-b") with a value of 8.15 Hz according to "Table 8" is not much of important, however, it should be considered while using the device. Regarding the resonant frequency of the inner basket subset, the matter seems a little different. Although, the extent of the displacement in the first mode is relatively high according to "Fig. 20-a", mode 4 ("Fig. 20-d") is more important here. As can be seen in this mode, the relative displacement has an almost large value compared to the other modes, which can represent the resonance in this mode. However, by comparing the natural frequency value of this mode and the normal working frequency range of the device ($5.83\ Hz$), it is determined that the possibility of resonance is negligible according to the calculations.

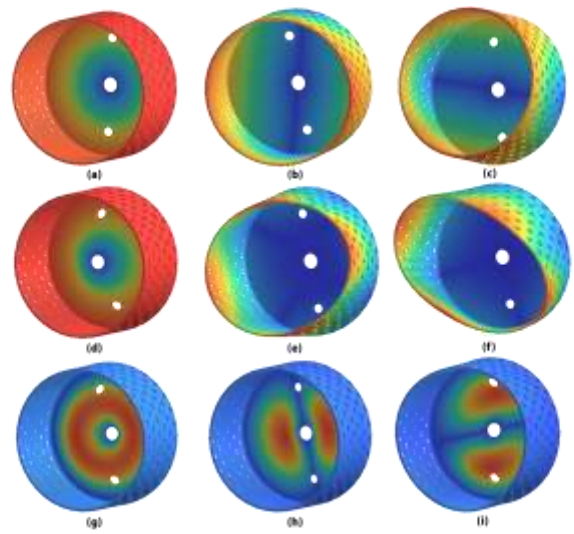

Fig. 20 The results of the modal analysis performed on the inner basket subset in the form of a colored contour of the relative maximum displacement: (a): mode 1, (b): mode 2, (c): mode 3, (d): mode 4, (e): mode 5, (f): mode 6, (g): mode 7, (h): mode 8, and (i): mode 9, (The range of changes from the minimum (blue) to the maximum (red) is the same for all of the items).

In overall, it should be stated that none of the calculated modes is equal to the working vibration frequency of the device. Although according to "Table 8", the value of the natural frequency obtained for mode 2 of the set has less difference than other values, since this value (8.15 Hz) is higher than the operating frequency of the device (5.83 Hz), reaching this value practically does not happen. Therefore, the margin of safety resulting from this comparison can be estimated at 40% after comparing the values in "Table 8" to the working conditions.

Table 7 Natural frequencies in the investigated modes of the inner basket subset

Mode No.	Natural frequency (Hz)	Mode No.	Natural frequency (Hz)
1	0.01	6	178.35
2	12.80	7	394.29
3	13.06	8	425.07
4	32.11	9	433.89
5	177.61		

By direct comparison of the natural frequency values in "Tables 8 & 9", it turned out that the lowest difference value (2.5 Hz) belonged to mode 8 of the set and mode 4 of the inner basket subset. The more important point is the small difference (3.64 Hz) between the natural frequency values of mode 3 for the desired set and the subset. A similar result can be seen for mode 2 as well. According to "Fig. 20-c", this vibration mode corresponds to displacement around a horizontal axis in the floor plane. Since such displacement and movement cannot be obtained directly by the normal operation of the device, it can be concluded that such vibration is far from expected.

3.2. Dynamic Behavior

The stress distribution and displacement results have been specifically discussed here. It should be noted that displacement in transient state dynamic analysis has been about the differential displacement, while kinematic displacement and motion analysis have not been directly analyzed here.

3.2.2. Particles

The contact points that occurred in the middle of the simulation process can be viewed in "Figs. 7 & 8" on the inner basket subset. Since the duration of feeding is considered from the beginning of the simulation to 8 s, the stress values obtained after the end of feeding duration have decreased according to data in "Fig. 10". The reason was the gradual exit of the particles in the inner basket. As "Fig. 9" shows, the usual range of stress values was between 0 and 4000 Pa. Considering the area of the target section in regions A to D ($0.004\ m^2$), the average force applied in these areas can be estimated between 0 and 16 N. The reason for the variations observed in this diagram ("Fig. 9") is the consecutive and random contacts of the particles with the target region, which caused fluctuations in the obtained value. The data obtained from this section proves that the analyzed set has the required mechanical strength against the dynamic stress caused by the particles.

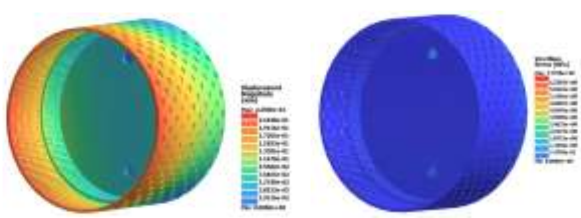

(a) **(b)**

Fig. 21 The displacements along with deformations: (a): and stress distribution, and (b): on the assembly in a critical state in the form of colored contours during the simulated process to check the dynamic behavior in transient state.

3.2.3. Transient State Dynamics

Figure 21 shows the results of the transient state dynamic analysis for the set. For simplicity in the display, the feeding section is hidden. According to "Fig. 21-a", the amount of displacement that occurred in the set is higher for peripheral and endpoints. In other words, the amount of displacement has increased by moving far from the engaged points which is natural. As can be seen in "Fig. 21-b", the amount of stress distribution caused in the subset of the external basket can be ignored, and what should be investigated more is the subset of the inner basket. Figure 22 shows the results of transient state dynamic analysis for the inner basket subset.

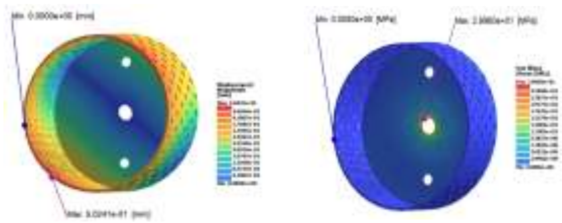

(a) **(b)**

Fig. 22 The displacements along with deformations: (a): and stress distribution, (b): on the inner basket subset in a critical state in the form of colored contours during the simulated process to check the dynamic behavior in transient state.

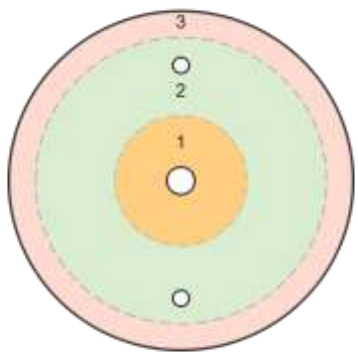

Fig. 23 Zoning of the bottom plate of the basket according to the significance of stress distribution.

As can be seen in the displacement distribution contour ("Fig 22-a"), the displacement is more in the peripheral and surrounding points than in the central and hole parts, although its amount is small and can be ignored. The distribution of the displacement that occurred on the bottom plane of the basket has also changed in layers. In other words, these changes have not been radial or circular. The same has been observed in a more regular way for the stress distribution ("Fig. 22-b"). In other words, the stress values around the central hole are the maximum, and the minimum values are at the peripheral points.

Also, on the bottom plane of the basket, the stress values in the outer ring are slightly higher than the inner ring. Regarding the stress distribution of the guiding rod holes, no special difference has been observed compared to the inner ring. Therefore, the stress distribution on the basket floor can be schematically divided into zones as displayed in "Fig. 23" in terms of importance.

Figure 24 shows the displacements in one of the peripheral points with critical conditions. The changes have occurred in short intervals and its high fluctuations are related to the lower values according to the diagram in "Fig. 24".

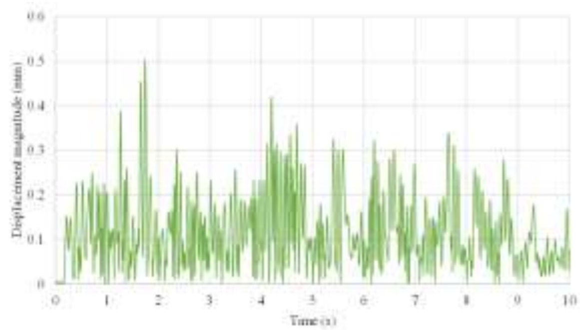

Fig. 24 Displacement variations during the simulation process on the critical point of the inner basket subset.

The graph also demonstrates the decreasing trend of the maximum values, which means the stabilization of its dynamic behavior after a certain period of time. The significant changes of the peaks have been relatively reduced after a period of 5 s and it can be said that the stability of the behavior is observed from this time onwards. Nevertheless, it should be noted that the reduction observed from the time interval of 9 s to the end is due to the interruption of the particles feeding at the time of 8 s, and it cannot be directly caused by variations in dynamic behavior and stability. A similar trend can be seen in the other way in "Fig. 25" regarding the changes of the stress value for the critical point in "Fig. 22-b".

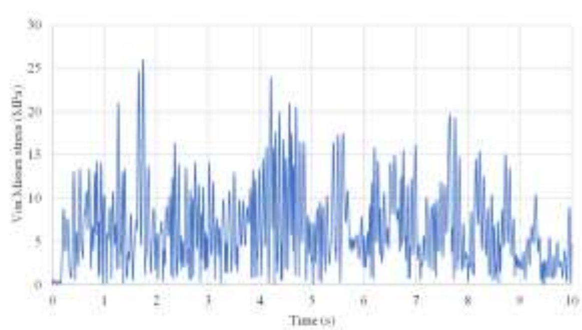

Fig. 25 Stress variations during the simulation process on the critical point of the inner basket subset.

Again, in this graph, the relative stability can be observed after $8\ s$. Therefore, the duration of stability of particle behavior is about $5.5\ s$ or 68% of the particle inlet time period. The maximum von Mises equivalent stress value has been below 20 MPa. Although this value is not significant from the mechanical point of view, it is useful for examining the dynamic behavior. Overall, the maximum displacement at the critical point of the inner basket subset has been 0.51 mm and the critical stress imposed on it is about 27 MPa according to the results. As a result, the mechanical strength of the assembly versus the stresses and strains caused by the operation of the device can be acceptable.

4 CONCLUSIONS

In this study, the structure and dynamic performance of the two-stage pusher centrifuge were analyzed. In this regard, the simulation process was done in three phases: modal analysis, particle behavior analysis, and transient state dynamics analysis. The results of the modal analysis showed that the safety margin obtained in the context of the occurrence of the resonance phenomenon due to the normal working vibration frequency of the device and the natural frequency of the assembly due to the change in the trend of linear and rotational inertial forces was 40%. In addition, based on the results of the transient dynamics analysis, the stability of the particle behavior was about 5.5 s or 68% of the particle feeding time, the maximum displacement at the critical point of the inner basket subset was 0.51 mm, and the critical stress on it was about 27 MPa; which means the acceptable mechanical strength of the assembly versus the stresses and strains caused by the operation of the device. What can be inferred based on the results of the analysis was the recommendation to maintain the maximum rotational motion ($36.68\frac{rad}{s}$) and no significant change in the particle feeding rate compared to the specified value ($0.56\frac{kg}{s}$). The following are also inferred according to the results:

- According to the modal analysis, the current rotating speed of the device would not lead to destructive or intensified vibrations.
- According to the modal analysis, the natural frequency of the desired set and the inner basket would not cause vibration problems in different modes.
- According to the transient state dynamic behavior analysis performed on the inner basket subset, the importance of stress distribution on the floor plane in the center has been identified as the most important and the least important was found to be in the middle ring.

- The range of displacements observed in the dynamic analysis of the transient state showed that the displacements around the assembly were in the range of small values and would not be problematic.
- Although the range of stress values and the resulting displacements is not considerable mechanically, increasing the feed rate, considering the linear and rotational inertial forces created, might lead to a change in the working vibration frequency of the device. Therefore, the possibility of resonance increases due to the differences obtained with the set and subset. Thus, it is suggested to increase the particle feed rate with caution and even after the experimental test if possible.
- Considering the required mechanical strength range, the use of lighter and even less strong materials could be appropriate for improving the performance of the device; Not only does it facilitate the process of fabrication and assembling the device, but also the inertial forces caused by the mass of the members and the tendency to run away from the center and damage to the bearings will be reduced.

REFERENCES

[1] Ergun, S., Orning, A. A., Fluid Flow through Randomly Packed Columns and Fluidized Beds. Industrial & Engineering Chemistry, Vol. 41, No. 6, 1949, pp. 1179-1184.

[2] Leung, W. W. F., Industrial Centrifugation Technology, McGraw-Hill Education, 1998.

[3] Romani Fernández, X., Nirschl, H., Multiphase CFD Simulation of a Solid Bowl Centrifuge. Chemical Engineering & Technology, Vol. 32, 2009, pp. 719-725.

[4] Stahl, S., Spelter, L. E., and Nirschl, H., Investigations on the Separation Efficiency of Tubular Bowl Centrifuges. Chemical Engineering & Technology, Vol. 31, No. 11, 2008, pp. 1577-1583.

[5] Ambler, C. M., The Theory of Scaling Up Laboratory Data for The Sedimentation Type Centrifuge, Journal of Biochemical and Microbiological Technology and Engineering, Vol. 1, No. 2, 1959, pp. 185-205.

[6] Pang, C., et al., Simulating Multiphase Flow in a Two-Stage Pusher Centrifuge Using Computational Fluid Dynamics, Frontiers of Chemical Science and Engineering, Vol. 6, No. 3, 2012, pp. 329-338.

[7] Bürger, R., F. Concha, Settling Velocities of Particulate Systems: 12, International Journal of Mineral Processing, Int J Miner Process, Vol. 63, 2001, pp. 115-145.

[8] Yan, F., Farouk, B., Numerical Simulations of Flows Inside a Partially Filled Centrifuge, Journal of Fluids Engineering, Vol. 125, 2003, pp. 1033.

[9] Anlauf, H., Recent Developments in Centrifuge Technology, Separation and Purification Technology,Vol. 58, No. 2, 2007, pp. 242-246.

[10] Wang, Y., et al., CFD Simulations of Membrane Filtration Zone in A Submerged Hollow Fibre Membrane Bioreactor Using a Porous Media Approach, Journal of Membrane Science, Vol. 363, No. 1, 2010, pp. 57-66.

[11] Ferry, J., Balachandar, S., A Fast Eulerian Method for Disperse Two-Phase Flow, International Journal of Multiphase Flow, Vol. 27, 2001, pp. 1199-1226.

[12] Nwogu, C., Design and Development of an Industrial Centrifuge for Small and Medium Scaled Industries, Innovative Systems Design and Engineering, 2015, pp. 6.

[13] Brouwers, J. J. H., Innovative Methods of Centrifugal Separation. Separations, Vol. 10, No. 3, 2023, pp. 181.

[14] Anlauf, H., Sorrentino, J. A., The Influence of Particle Collective Characteristics on Cake Filtration Results, Chemical Engineering & Technology, Vol. 27, No. 10, 2004, pp. 1080-1084.

[15] Bentz, M., Hartmetz, O., and W., Stahl, Particle Destruction Effects in Pusher Centrifuges during Solids-Liquid Separation, Chemical Engineering & Technology, Vol. 27, No. 10, 2004, pp. 1075-1080.

[16] Deshmukh, S., Joshi, J., Flow Visualization and Three-Dimensional CFD Simulation of the Annular Region of an Annular Centrifugal Extractor, Industrial & Engineering Chemistry Research - IND Eng Chem Res, 2007, pp. 47.

[17] Leung, W. W. F., Shapiro, A. H., Improved Design of Conical Accelerators for Decanter and Pusher Centrifuges, Filtration & Separation, Vol. 33, No. 8, 1996, pp. 735-738.